LOW-PROFILE OPEN-SLOT ANTENNA WITH THREE BRANCH SLOTS FOR TRIPLE-WIDEBAND LTE OPERATION IN THE METAL-FRAMED SMARTPHONE

Kin-Lu Wong and Ya-Jyun Li
Department of Electrical Engineering, National Sun Yat-Sen University, Kaohsiung 80424, Taiwan; Corresponding author: wongkl@ema.ee.nsysu.edu.tw

Received 4 March 2015

ABSTRACT: *A low-profile open-slot antenna capable of providing a triple-wideband LTE operation for the metal-framed smartphone is presented. The antenna has a low profile of 7 mm and can fit in a narrow region between the metal frame and the display panel of the metal-framed smartphone. The antenna comprises three branch slots sharing a same opening disposed at the top or bottom edge of the casing of the smartphone. Two branch slots are excited using a U-shape microstrip feedline with wideband matching circuits embedded therein while the third-branch slot is excited parasitically. With the proposed feeding arrangement, the antenna provides the triple-wideband LTE operation to cover the low band of 698–960 MHz, middle band of 1710–2690 MHz, and high band of 3400–3800 MHz. Details of the proposed open-slot antenna are presented and discussed.* © 2015 Wiley Periodicals, Inc. Microwave Opt Technol Lett 57:2231–2238, 2015; View this article online at wileyonlinelibrary.com. DOI 10.1002/mop.29320

Key words: *mobile antennas; open-slot antennas; small antennas; triple-wideband; antennas; LTE antennas*

1. INTRODUCTION

Recently, the smartphone with a large display is becoming very attractive. For such smartphones, the region between the display panel and the top or bottom edge of the casing thereof becomes very narrow and is usually less than 10 mm. Furthermore, as the modern smartphone also becomes very slim with a thin thickness, a metal frame is attractive to be disposed around the casing of the smartphone to enhance its mechanical robustness [1,2]. With the presence of the metal frame and the narrow available region between the metal frame and the display panel, it is a great design challenge to achieve a wideband or multiband antenna embedded therein.

In this article, we present a low-profile open-slot antenna capable of providing a triple-wideband LTE operation in the 698–960, 1710–2690, and 3400–3800 MHz [3–6] for the metal-framed smartphone. The antenna is a three-branch open slot with its opening disposed at the top or bottom edge of the casing of the smartphone. The three-branch open slot is configured to have a low profile of 7 mm, which makes it promising to fit in the narrow region between the metal frame and the display panel. Wideband operation of the antenna in the desired three operating bands is obtained with the aid of wideband matching circuits in the microtrip feedline feeding the antenna. The configuration and operating principle of the antenna will be described in detail in this study. Experimental results of the fabricated antenna will also be presented and discussed.

In addition to the wideband and multiband operations of the proposed antenna, it should be noted that the low profile of 7 mm for the proposed antenna is better than many reported LTE antennas that can cover at least 698–960 and 1710–2690 MHz bands for the smartphone or the tablet computer application [7–12]. Also, owing to the presence of the metal frame, large effects on many of the reported LTE antennas [7–12] are expected, which makes them not promising for applications in the metal-framed smartphone.

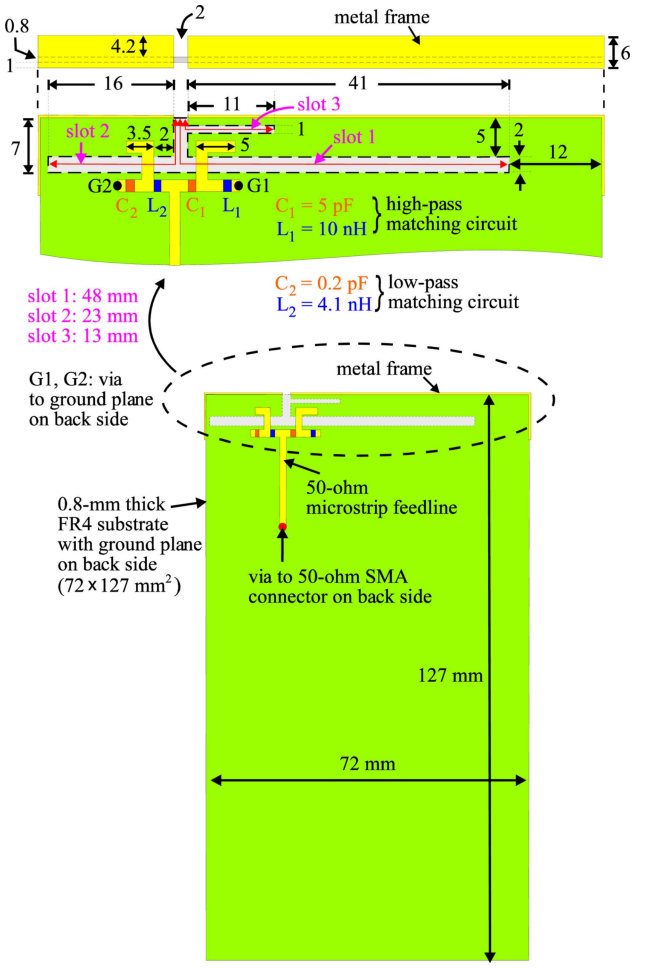

Figure 1 Geometry of the low-profile triple-wideband open-slot antenna for the metal-framed LTE smartphone. [Color figure can be viewed in the online issue, which is available at wileyonlinelibrary.com]

It is also noted that, for the open slot antenna, the metal portion around the slot can be reused to accommodate the associated electronic elements [13,14]. This makes it attractive to achieve compact integration of the antenna inside the smartphone. In this study, the case of the antenna with a nearby USB connector in the 7-mm narrow region between the metal frame and the display panel is also studied.

2. PROPOSED ANTENNA

2.1. Antenna Configuration

Figure 1 shows the geometry of the proposed open-slot antenna for the metal-framed LTE smartphone. The antenna comprises a three-branch open slot, which is embedded on the ground plane printed on the back side of a 0.8-mm thick FR4 substrate of relative permittivity 4.4 and loss tangent 0.02. The dimensions of the FR4 substrate are selected to be 72 × 127 mm^2, which is considered as the circuit board of a 5.5-inch smartphone. The three-branch open slot occupies a narrow region of 7 mm to the short edge (top edge in Fig. 1) of the FR4 substrate, at which a metal plate of width 6 mm is connected orthogonally to the ground plane. The metal plate is used to model the metal frame of the smartphone. Note that for practical applications, the metal frame is generally disposed around all the boundary of the

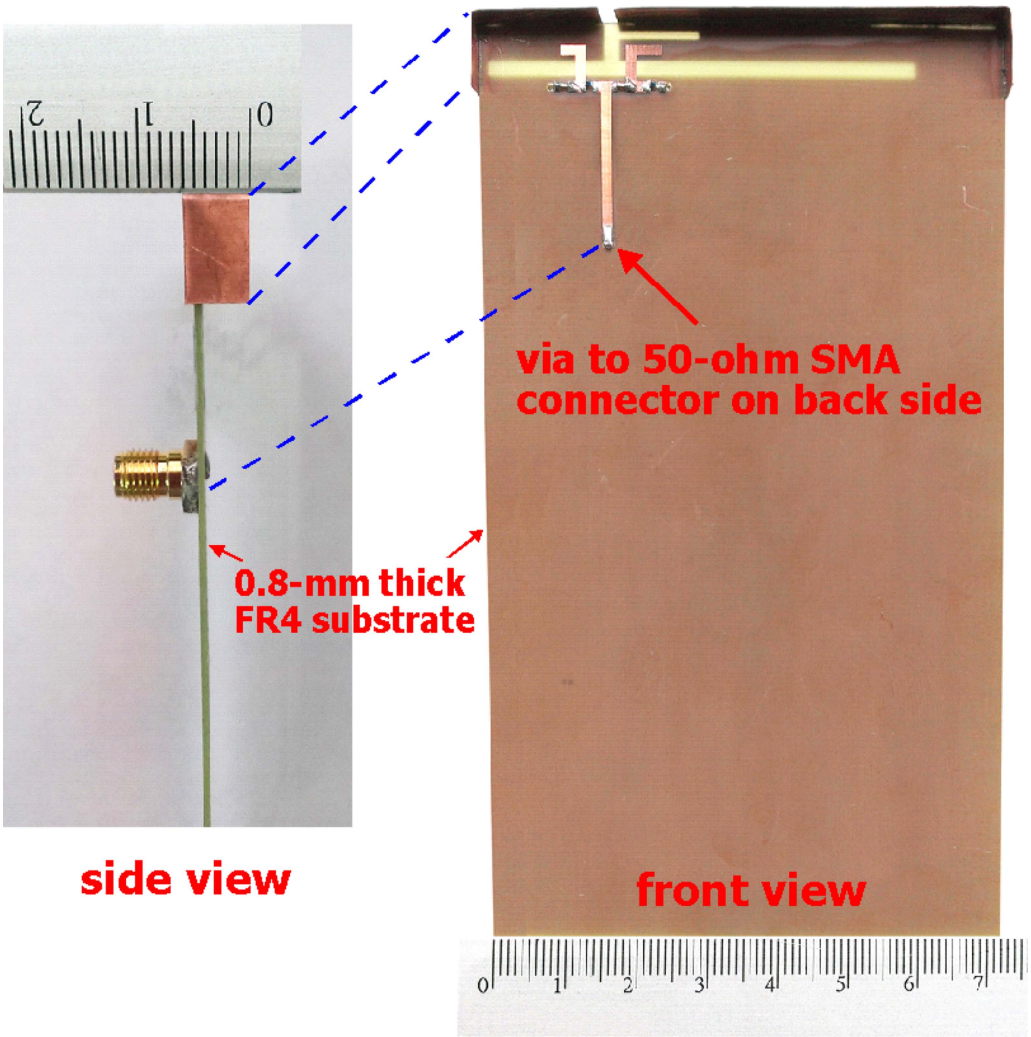

Figure 2 Photos of the fabricated antenna. [Color figure can be viewed in the online issue, which is available at wileyonlinelibrary.com]

casing of the smartphone. Here, to simplify the structure in the study, only the metal frame around the top region where the open-slot antenna is located is added. It is expected that the obtained results in this study will be generally the same as those obtained for the case of using a complete metal frame around the FR4 substrate.

To understand the proposed antenna more clearly, the photos of the fabricated antenna are shown in Figure 2. Note that at the metal frame, there is a gap of width 2 mm. The gap is at the position of the opening of the three-branch open slot, which provides three open slots of different lengths. Slot 1 is the longest open slot with a length of 48 mm and a width of 2 mm. Slot 2 has a length of 23 mm and a width of 2 mm. Slot 3 is the shortest open slot with a length of 13 mm. Note that slot 1 and 2 are directly excited by a U-shape microstrip feedline while slot 3 is parasitically excited. The width of the horizontal section of slot 3 is selected to be 1 mm only, smaller than that of slot 1 and 2.

Slot 1, 2, and 3 share a same opening of width 2 mm at the metal frame. The lengths of slot 1 and 2 are about 0.14 wavelength at 0.9 and 1.8 GHz, respectively, while that of slot 3 is about 0.16 wavelength at about 3.6 GHz. Although their lengths are much less than 0.25 wavelength, the three slots can contribute their fundamental resonant modes at about 0.9, 1.8, and 3.6 GHz, in the desired low band, middle band, and high band of the antenna. The decrease in the required resonant length is owing to the FR4 substrate loading on the open slot [15,16], which is advantageous for the open-slot antenna to achieve a reduced size for the smartphone application.

In addition to adjust the tuning-stub's lengths of the two branches of the U-shape microstrip feedline to achieve improved impedance matching of the antenna, two matching circuits are embedded to effectively widen the operating bandwidth of the antenna. With the aid of the high-pass matching circuit formed by the chip capacitor C_1 (5 pF) and the chip inductor L_1 (10 nH) in the first branch of the U-shape microstrip feedline, enhanced bandwidth of the antenna's low band can be obtained. Conversely, with the aid of the low-pass matching circuit formed by the chip capacitor C_2 (0.2 pF) and chip inductor L_2 (4.1 nH) in the second branch of the U-shape microstrip feedline, wide middle and high bands of the antenna can be obtained. That is, the high-pass and low-pass matching circuits formed as the wideband matching circuits embedded in the U-shaped microstrip feedline. The proposed antenna with the wideband matching circuits can hence provide a triple-wideband LTE operation to cover the 698–960/1710–2690/3400–3800 MHz bands.

2.2. Operating Principle

To analyze the operating principle of the antenna, Figure 3 shows the simulated return loss for the proposed antenna and

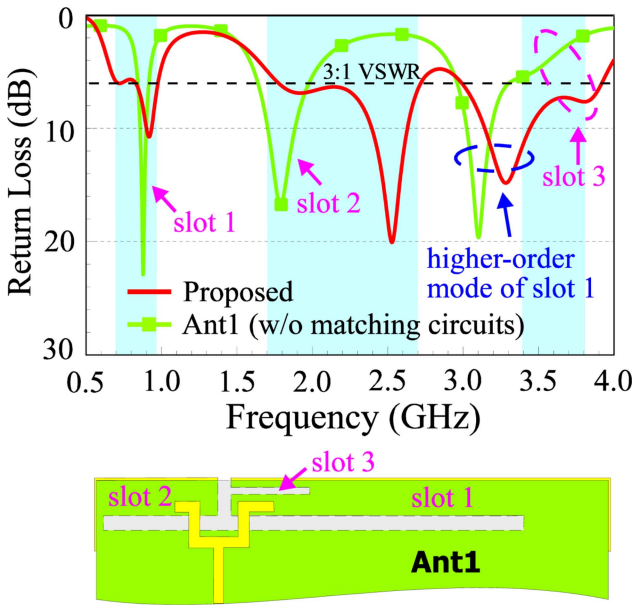

Figure 3 Simulated return loss for the proposed antenna and Ant1 (no matching circuits in the U-shape microstrip feedline). [Color figure can be viewed in the online issue, which is available at wileyonlinelibrary.com]

Ant1. The geometry of Ant1 (no matching circuits in the U-shape microstrip feedline) is also shown in the figure. The simulated results are obtained using the full-wave electromagnetic field simulator HFSS version 15 [17]. It is seen that the proposed antenna can cover three wide operating bands for the LTE operation (see the three shaded frequency regions in the figure). For Ant1, its operating bandwidths are far from covering the desired three LTE bands. However, the three branch slots of the proposed antenna can contribute resonant modes for the desired low, middle, and high bands. From the results for Ant1 in the figure, the resonant modes at about 0.9 and 1.8 GHz are, respectively, the fundamental or quarter-wavelength resonant modes of slot 1 and 2 [18–21]. The resonant mode at about 3.1 GHz is the higher-order resonant mode of slot 1. The resonant mode at about 3.6 GHz, although with poor impedance matching, is contributed by slot 3. The confirmation of the slot resonant mode excitation will be discussed later with the aid of Figure 8 in which the excited electric field, and surface current distributions will be presented.

To show the effects of the high-pass matching circuit (C_1 and L_1) embedded in microstrip feedline, Figure 4 shows the simulated return loss for Ant1 and Ant2. The antenna structure of Ant2, which is Ant1 with the presence of C_1 and L_1, is also shown in the figure. It is clearly seen that the antenna's low band shows a dual-resonance behavior, and its bandwidth is greatly widened. Conversely, the resonant modes at higher frequencies are almost not affected by the high-pass matching circuit.

To show the impedance matching improvement in the antenna's low band, Figure 5 shows the simulated input impedance on the Smith chart for Ant1 (curve 1), Ant2 (curve 2), and proposed antenna (curve 3) in the frequency range of 650–1000 MHz. Within the 3:1 VSWR circle, curve 1 shows a simple curve, suggesting that a single resonant mode is excited while curve 2 shows a loop-type curve, indicating that a dual-resonance excitation occurs. It is also seen that curve 2 and 3 show very small variations. This suggests that the adding of the low-pass matching circuit (C_2 and L_2) has very small effects on the antenna's low-band matching, which is advantageous for adjusting the antenna's impedance matching in its low, middle, and high bands.

Effects of the low-pass matching circuit (C_2 and L_2) are discussed with the aid of Figure 6, in which the simulated return

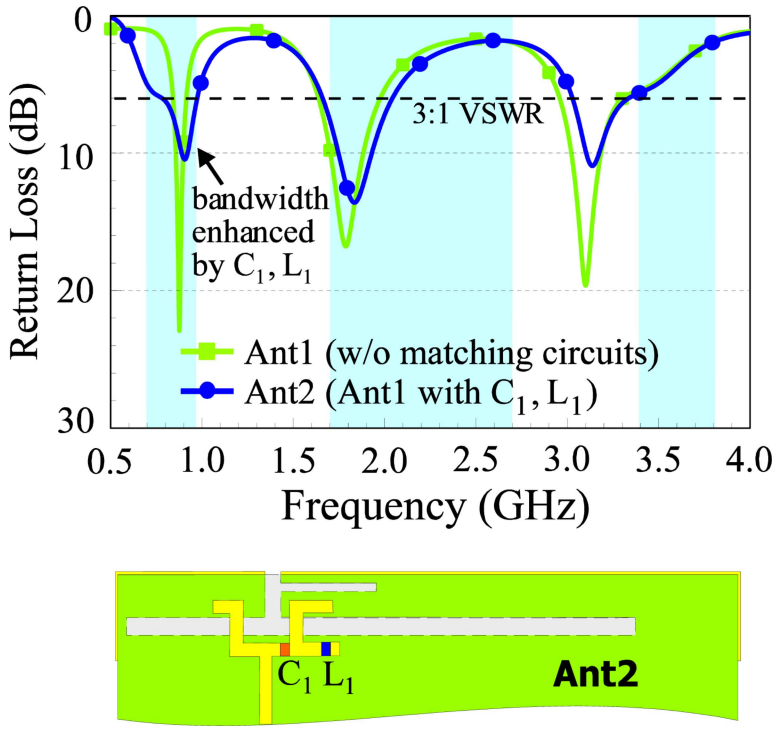

Figure 4 Simulated return loss for Ant1 and Ant2 (Ant1 with C_1 and L_1). [Color figure can be viewed in the online issue, which is available at wileyonlinelibrary.com]

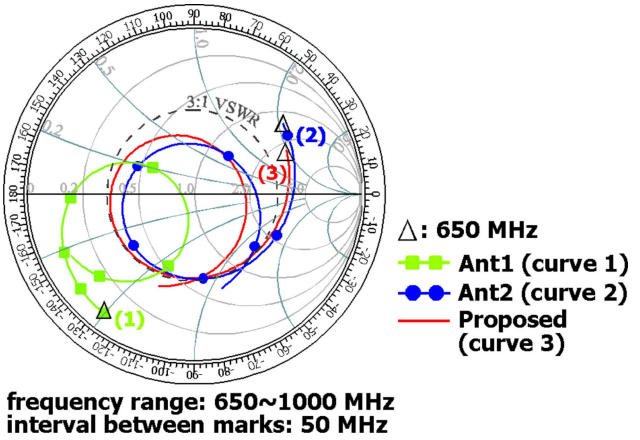

Figure 5 Simulated input impedance on the Smith chart for Ant1 (curve 1), Ant2 (curve 2), and proposed antenna (curve 3) in the frequency range of 650–1000 MHz. [Color figure can be viewed in the online issue, which is available at wileyonlinelibrary.com]

loss for Ant1 and Ant3 is presented. The antenna structure of Ant3, which is Ant1 with the presence of C_2 and L_2, is also shown in the figure. From the results, an additional mode is generated at about 2.5 GHz, which combines with the resonant mode at about 1.8 GHz to greatly widen the antenna's middle band. In addition, the resonant mode at about 3.8 GHz contributed by slot 3 is excited with good impedance matching while the higher-order resonant mode contributed by slot 1 is shifted from about 3.1 to 3.3 GHz. The two modes lead to much better impedance matching for frequencies in the antenna's high band. Furthermore, it is seen that the antenna's low band is slightly affected by the presence of the low-pass matching circuit. Again, this behavior makes it convenient for the antenna to achieve good impedance matching in its three operating bands.

To see more clearly the impedance matching improvement in the antenna's middle and high bands, the simulated input impedance on the Smith chart for Ant1 (curve 1), Ant3 (curve 2), and

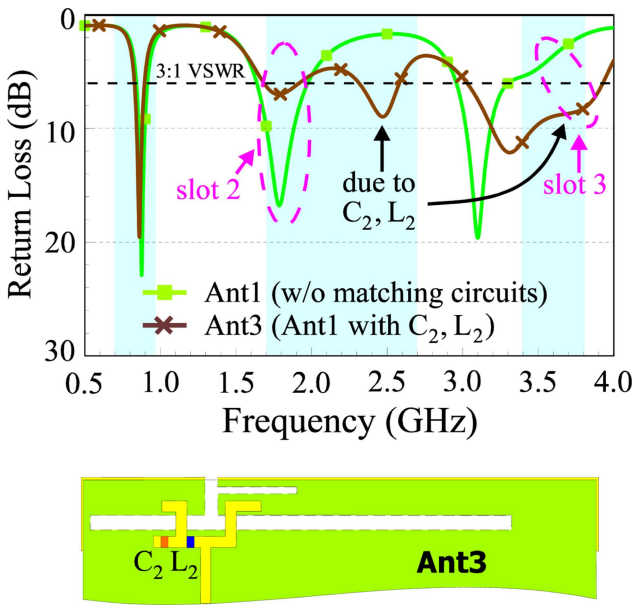

Figure 6 Simulated return loss for Ant1 and Ant3 (Ant1 with C_2 and L_2). [Color figure can be viewed in the online issue, which is available at wileyonlinelibrary.com]

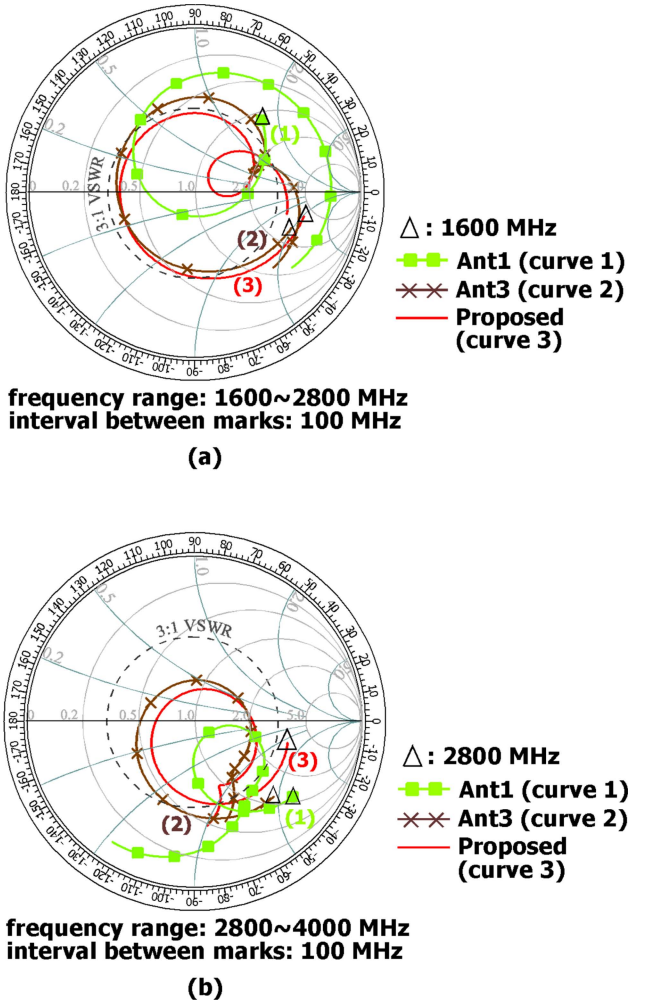

Figure 7 Simulated input impedance on the Smith chart for Ant1 (curve 1), Ant3 (curve 2), and proposed antenna (curve 3) in the frequency ranges of (a) 1600–2800 MHz and (b) 2800–4000 MHz. [Color figure can be viewed in the online issue, which is available at wileyonlinelibrary.com]

proposed antenna (curve 3) in the frequency ranges of 1600–2800 MHz and 2800–4000 MHz are, respectively, shown in Figures 7(a) and 7(b). Similar to the results in Figure 5, within the 3:1 VSWR, curve 1 indicates a single-resonant mode excitation, and curve 2 is a loop-like curve, suggesting a dual-resonance excitation in the antenna's middle band. In Figure 7(b), similarly, a loop-type curve is obtained for curve 2 (Ant3) within the 3:1 VSWR, indicating much improved impedance matching for frequencies in the antenna's desired high band. In addition, in Figures 7(a) and 7(b), small variations between curve 2 and 3 are also seen. This suggests that the adding of the high-pass matching circuit (C_1 and L_1) has small effects on the impedance matching of the middle and high bands.

To confirm the excitation of the slot resonant modes, Figure 8 shows the simulated electric field and surface current distributions for the proposed antenna. At 0.7 GHz, it is seen that strong electric fields are excited in slot 1, and symmetric surface currents around the boundary of slot 1 are also seen. In addition, the excited electric fields in slot 1 gradually increase from the closed end to the open end thereof, indicating that smooth variations of the electric field distribution occur in slot 1. These observations indicate that a quarter-wavelength slot resonant

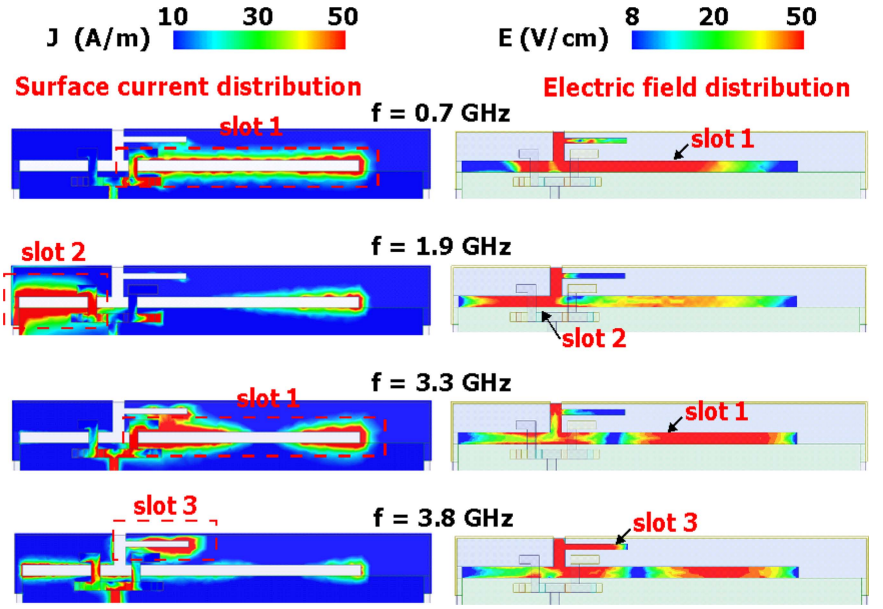

Figure 8 Simulated electric field and surface current distributions for the proposed antenna. [Color figure can be viewed in the online issue, which is available at wileyonlinelibrary.com]

mode is excited in slot 1. This also suggests that the antenna's low band is mainly contributed by slot 1.

At 1.9 GHz, strong electric fields are seen in slot 2. Symmetric surface currents around the boundary of slot 2 are also seen. The distributions of the electric field and surface current are similar to those observed at 0.7 GHz in slot 1. Hence, it can also be confirmed that a quarter-wavelength slot resonant mode is excited in slot 2. At 3.3 GHz, strong electric fields are also excited in slot 1. However, a null electric field is seen in slot 1. The excited surface currents around the boundary of slot 1 also show corresponding current nulls. This indicates that the higher-order slot resonant mode is excited at 3.3 GHz. At 3.8 GHz, strong electric fields in slot 3 and symmetric surface currents around slot 3 are observed, which indicates that a quarter-wavelength slot resonant mode is excited. The observations in Figure 8 confirm that the antenna's low, middle and high bands are, respectively, contributed by the resonant modes contributed by slot 1, 2, and 3.

3. EXPERIMENTAL RESULTS AND DISCUSSION

3.1. Experimental Results

The proposed antenna was also fabricated (see the photos shown in Fig. 2) and experimentally studied. Figure 9 shows the measured and simulated return loss of the fabricated antenna. The results show agreement between the measured data and simulated results. The measured return loss shows acceptable impedance matching (3:1 VSWR) for frequencies in the antenna's low, middle, and high bands for the triple-wideband LTE operation.

Figure 10 shows the measured and simulated antenna efficiency for the fabricated antenna. The radiation characteristics of the antenna were measured in a far-field anechoic chamber. The measured data also generally agree with the simulated results. Note that the measured antenna efficiency includes the mismatching losses. The measured antenna efficiency varies in the ranges of about 42–58% in the low band, 51–78% in the middle band, and 71–85% in the high band. The antenna

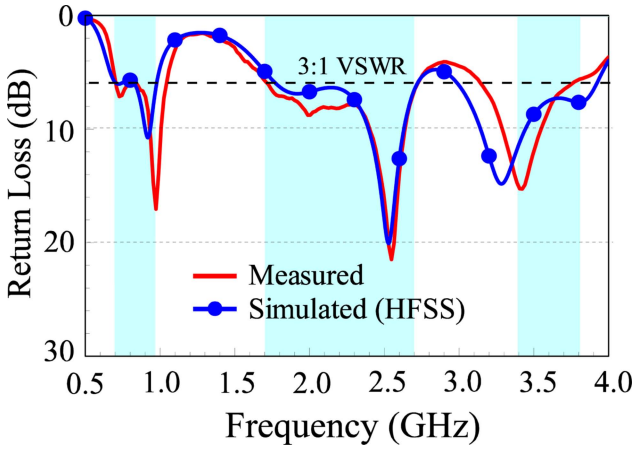

Figure 9 Measured and simulated return loss for proposed antenna. [Color figure can be viewed in the online issue, which is available at wileyonlinelibrary.com]

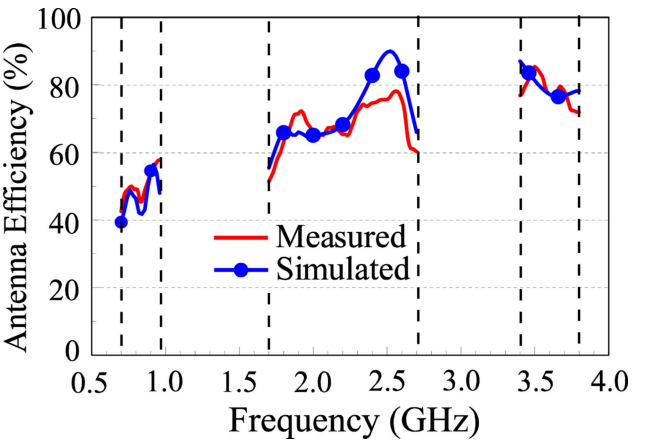

Figure 10 Measured and simulated antenna efficiency for the proposed antenna. [Color figure can be viewed in the online issue, which is available at wileyonlinelibrary.com]

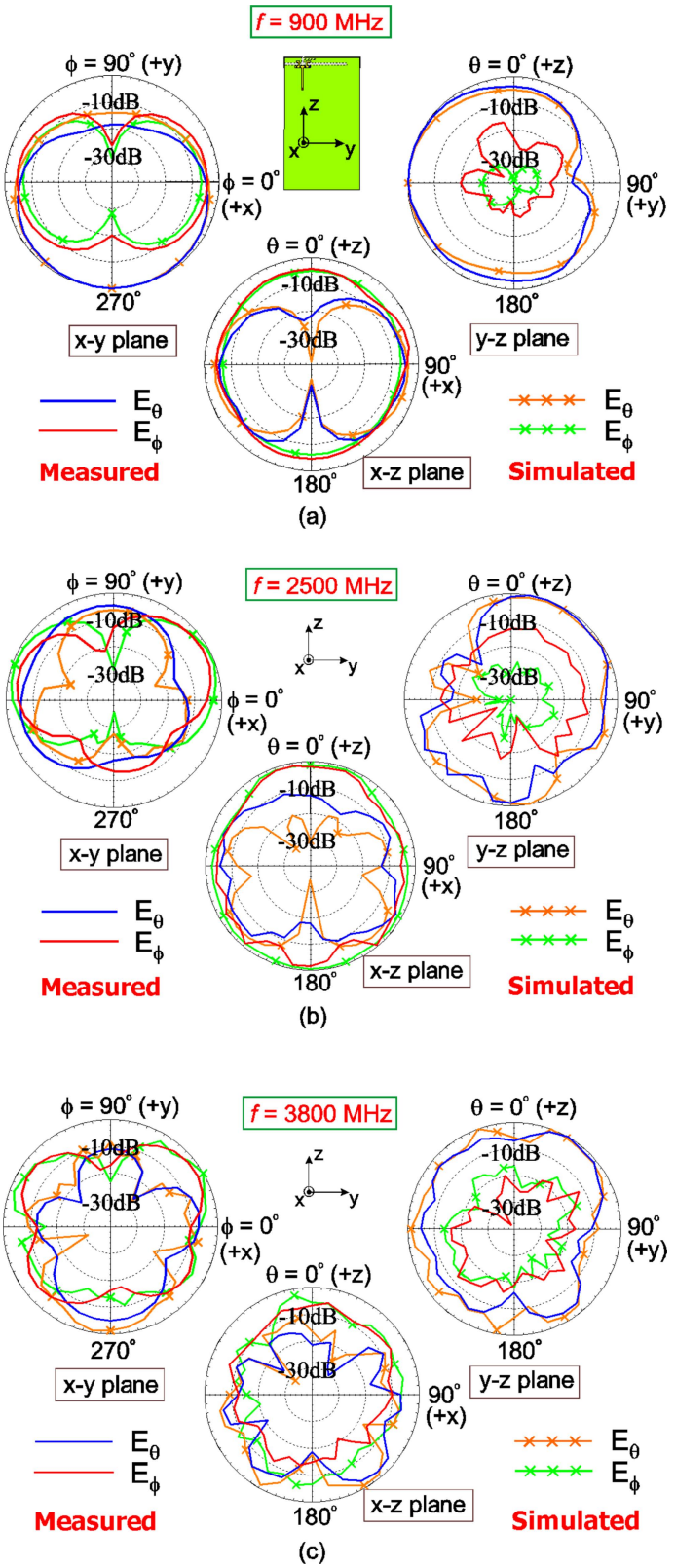

Figure 11 Measured and simulated radiation patterns for the proposed antenna. [Color figure can be viewed in the online issue, which is available at wileyonlinelibrary.com]

efficiency in the low band is better than 40% while that in the middle and high bands is better than 50%. The obtained antenna efficiencies are acceptable for practical mobile communication applications [10].

Figure 11 shows the measured and simulated radiation patterns for the proposed antenna. Three representative frequencies at 900, 2500, and 3800 MHz are shown. From the radiation patterns in the *x-y* plane (azimuthal plane) and *y-z* plane (elevation

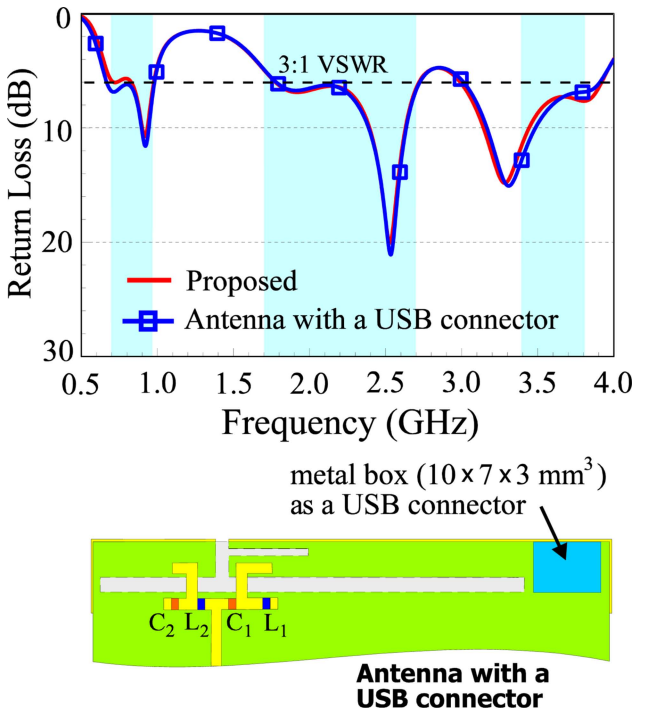

Figure 12 Simulated return loss for the proposed antenna with and without a nearby USB connector. [Color figure can be viewed in the online issue, which is available at wileyonlinelibrary.com]

plane parallel to the system ground plane) at 900 MHz (a representative frequency in the low band), stronger radiation in the $-y$ direction is seen. This is mainly related to the structure of slot 1 that its opening where strong electric fields occur is to the $-y$ direction of structure. In the x-z plane (elevation plane orthogonal to the system ground plane), symmetric radiation pattern is seen. This behavior is reasonable, as the antenna structure is planar in the y-z plane. Hence, the radiation will be symmetric in both the $+x$ and $-x$ directions.

At 2500 MHz (a representative frequency in the middle band), stronger radiation is seen in the $+y$ direction as seen from the radiation patterns in the x-y and y-z planes. This is also related to the structure of slot 2 that its opening where strong electric fields occur is to the $+y$ direction of the structure. The radiation pattern in the x-z plane is also generally symmetric with respect to the system ground plane. At 3800 MHz (a representative frequency in the high band), stronger radiation in the $-y$ direction is seen in the x-y and y-z plane, similar to the observation at 900 MHz. This behavior is also related to the structure of slot 3 whose opening is to the $-y$ direction. For the pattern in the x-z plane, symmetric radiation patterns with respect to the system ground plane is again observed. From the obtained radiation patterns at all frequencies, as there are no nulls in the radiation at all directions, the antenna can provide acceptable coverage for mobile communication applications.

3.2. Antenna With a Nearby USB Connector

The case of the antenna integrated with a nearby USB connector is studied. Figure 12 shows the simulated return loss for the proposed antenna with and without a nearby USB connector. As shown in the figure, the USB connector is added close to the closed end of slot 1 and integrated in the 7-mm narrow region between the metal frame and the display panel. Note that in the study, the USB connector is modeled as a metal box of 10 $\times$ 7 $\times$ 3 mm^3. The results show that very small variations in the return loss are seen for the antenna with and without the USB connector. This indicates that the proposed antenna can be closely integrated with nearby electronic elements in practical applications.

4. CONCLUSION

A low-profile (7 mm) open-slot antenna with three branch slots for triple-wideband LTE operation in the metal-framed smartphone has been proposed. The antenna's triple-wideband operation is mainly controlled by the three branch slots, and the wideband operation is obtained by the wideband feed structure consisting of a U-shape microstrip feedline and wideband matching circuits embedded therein. The operating principle of the antenna has been addressed. Acceptable radiation characteristics for frequencies in the antenna's three wide operating bands have been obtained. With a low profile of 7 mm, the antenna is promising to be disposed in the narrow region between the metal frame and display panel of the metal-framed smartphone.

REFERENCES

1. B. Yuan, Y. Cao, G. Wang, and B. Cui, Slot antenna for metal-rimmed mobile handsets, IEEE Antennas Wireless Propag Lett 11 (2012), 1334–1337.
2. J Zhong, K.K Chen, and X Sun, A novel multi-band antenna for mobile phone with metal frame, In: 2012 International Conference on Wireless Communications, Networking and Mobile Computing, Shanghai, China, 2012, pp. 1–4.
3. I Poole, LTE frequency bands and spectrum allocations, available at http://www.radio-electronics.com/
4. K.L. Wong and T.W. Weng, Small-size triple-wideband LTE/WWAN tablet device antenna, IEEE Antennas Wireless Propag Lett 12 (2013), 1516–1519.
5. K.L. Wong and T.W. Weng, Small-size triple-wideband LTE tablet device antenna with a wideband feed structure formed by integrated matching network, Microwave Opt Technol Lett 56 (2014), 2507–2512.
6. K.L. Wong and Z.G. Liao, Passive reconfigurable triple-wideband antenna for LTE tablet computer, IEEE Trans Antennas Propag 63 (2015), 901–908.
7. K.L. Wong and L.Y. Chen, Small-size LTE/WWAN tablet device antenna with two hybrid feeds, IEEE Trans Antennas Propag 62 (2014), 2926–2934.
8. K.L. Wong and C.Y. Tsai, Small-size stacked inverted-F antenna with two hybrid shorting strips for the LTE/WWAN tablet device, IEEE Trans Antennas Propag 62 (2014), 3962–3969.
9. Y.L. Ban, S.C. Sun, P.P. Li, J.L. W. Li, and K. Kang, Compact eight-band frequency reconfigurable antenna for LTE/WWAN tablet computer applications, IEEE Trans Antennas Propag 62 (2014), 471–475.
10. K.L. Wong and M.T. Chen, Small-size LTE/WWAN printed loop antenna with an inductively coupled branch strip for bandwidth enhancement in the tablet computer, IEEE Trans Antennas Propag 61 (2013), 6144–6151.
11. Y.L. Ban, J.H. Chen, S. Yang, J.L.W. Li, and Y.J. Wu, Low-profile printed octa-band LTE/WWAN mobile phone antenna using embedded parallel resonant structure, IEEE Trans Antennas Propag 61 (2013), 3889–3894.
12. J.H. Lu and F.C. Tsai, Planar internal LTE/WWAN monopole antenna for tablet computer application, IEEE Trans Antennas Propag 61 (2013), 4358–4363.
13. K.L. Wong, P.W. Lin, and C.H. Chang, Simple printed monopole slot antenna for penta-band WWAN operation in the mobile handset, Microwave Opt Technol Lett 53 (2011), 1399–1404.

14. K.L. Wong and P.W. Lin, Integration of monopole slot and monopole strip for internal WWAN handset antenna, Microwave Opt Technol Lett 54 (2012), 1718–1723.
15. C.I. Lin and K.L. Wong, Printed monopole slot antenna for internal multiband mobile phone antenna, IEEE Trans Antennas Propag 55 (2007), 3690–3697.
16. K.L. Wong and L.C. Lee, Multiband printed monopole slot antenna for WWAN operation in the laptop computer, IEEE Trans Antennas Propag 57 (2009), 324–330.
17. http://www.ansys.com/products/hf/hfss/, ANSYS HFSS.
18. H. Wang, M. Zheng, and S.Q. Zhang, Monopole slot antenna, U.S. Patent No. 6618020 B2, 2003.
19. P.L Sun, H.K Dai, and C.H Huang, Dual band slot antenna with single feed line, US Patent No. 6677909 B2, 2004.
20. Z. Liu and K. Boyle, Bandwidth enhancement of a quarter-wavelength slot antenna by capacitive loading, Microwave Opt Technol Lett 51 (2009), 2114–2116.
21. F.H. Chu and K.L. Wong, Simple folded monopole slot antenna for penta-band clamshell mobile phone application, IEEE Trans Antennas Propag 57 (2009), 3680–3684.

THE CHARACTERISTICS OF THE DIPOLE ESPAR ANTENNA USING THE CROSS-COPLANAR WAVEGUIDE FEED

Jae-Sung Park,[1] Seung-Hwan Lee,[2] and Hak-Keun Choi[1]
[1] Department of Electronic Engineering, Dankook University, Korea; Corresponding author: hkchoi@dankook.ac.kr
[2] Electronics and Telecommunications Research Institute (ETRI), Daejeon, Korea

Received 5 March 2015

ABSTRACT: *This article suggests a dipole electrically steerable parasitic array radiator (ESPAR) antenna that uses a crossed coplanar waveguide (CPW) transmission line that can be applied to beamspace multi-input-multioutput communication. The dipole antenna, which uses a vertically standing cylindrical structure, requires a feeding method that uses coaxial cable as the cable is connected inside the cylinder. As a result, it has the shortcoming of having to use cable with a limited diameter due to the cylindrical diameter as well as weak structure because of the flexible characteristic of coaxial cable. The antenna suggested in this article is rigid because it has a crossed PCB structure and it also has easier impedance matching than the cable feeding method because has a CPW transmission line. Moreover, the crossed CPW dipole ESPAR antenna turned out to have a radiation pattern similar to a dipole ESPAR antenna composed of a cylindrical structure.*
 Microwave Opt Technol Lett 57:2238–2242, 2015; View this article online at wileyonlinelibrary.com. DOI 10.1002/mop.29319

Key words: *beamspace multi-input-multioutput; electrically steerable parasitic array radiator antenna; cross-coplanar waveguide transmission line; cross-CPW dipole ESPAR antenna*

1. INTRODUCTION

Users provided with diverse communication contents demands faster speeds and those who provide contents put a great value on the efficiency of diverse information transfers. A variety of studies on communication systems that are suitable for the needs of the providers and users have been conducted, and the multi-input-multioutput (MIMO) communication system is especially in the limelight [1]. When a signal is transmitted using multiple antennas in the communication method of the MIMO system, the channel capacity increases according to the number of antennas. However, a conventional MIMO system where channel capacity is increased by adding more antennas has increased electricity consumption and system complexity because the RF chain increases along with the number of antennas. Moreover, it occupies a large amount of space because the distance between antennas should be secured to decrease mutual coupling among the antennas. The beamspace MIMO system was suggested for the purpose of solving this problem. Currently, a number of studies are in progress that examines the single RF chain communication method using electrically steerable parasitic array radiator (ESPAR) antennas composed of one driven element and multiple surrounding parasitic elements, instead of increasing the number of antennas for more diverse data transfer [2–5]. In a beamspace MIMO system, data can be transmitted by mapping the data signal to the orthogonal basis pattern of the radiation pattern. Here, the orthogonal basis pattern can be obtained by calculating the correlation of the radiation pattern. According to the previous literature [6], an orthogonal basis pattern that is suitable for communication is determined by following the distance between the driven element and the parasitic element [6,7]. The arraying distance in the suggested antenna is $\lambda/16$ and the impedance matching becomes difficult as the arraying distance between each element becomes narrower as it increases the mutual coupling characteristics [8].

Hence, this article improve the degradation of antenna characteristics that comes from the narrowing element's distance by applying a cross-CPW feeding structure to a dipole ESPAR antenna using its feature of adjustable antenna impedance.

2. ESPAR ANTENNA IN BEAMSPACE MIMO

In a beamspace MIMO system, the radiation pattern changes when the ESPAR antenna's reactance value changes as a stream is allowed to the driven element and another stream is allowed to the parasitic element. Computing the correlation of the changed radiation pattern shows that it is composed of the sum of the orthogonal basis patterns. Hence, it is possible to form spatial multiplexing with different radiation patterns by adjusting the reactance values that are allowed to the parasitic elements of ESPAR antennas [6].

Figure1 shows a five-element dipole ESPAR antenna. In an ESPAR antenna, the reactance circuit is connected to multiple parasitic elements. The radiation pattern changes when loading the reactance that is connected to a parasitic element changes.

The radiation pattern of a dipole ESPAR antenna can be expressed as formula (1). M is the number of elements, i_m is the current in the element and d is the distance between the driven element and the parasitic element.

$$P(\theta,\phi)=\sum_{m=0}^{M-1} i_m e^{jkd_m \sin\theta\cos(\phi-\phi_m)} \quad M=5 \tag{1}$$

In a dipole ESPAR antenna, the induced current of the parasitic element is generated by the current in the driven element.

$$\begin{gathered} i = v_s(Z+X)^{-1}u \\ \mathrm{X}=\mathrm{diag}[R_0,\ jx1,\ jx2,\cdots\cdots,jx_{M-1} \\ u=[1\ 0\cdots\ 0]^T \end{gathered} \tag{2}$$

Current can be expressed as formula (2). Z represents mutual impedance, X is the reactance value of each element, v_s is the signal allowed to the driven element, and u is a vector with M entities [7].